Modeling and simulating optical MEMS using Chatoyant

Timothy P. Kurzweg[a], Steven P. Levitan[*a], Philippe J. Marchand[b], Jose A. Martinez[a], Kurt R. Prough[a], Donald M. Chiarulli[c]

[a]Department of Electrical Engineering, University of Pittsburgh

[b]Department of Electrical and Computer Engineering, University of California/San Diego

[c]Department of Computer Science, University of Pittsburgh

ABSTRACT

The use of MEMs technology has enabled the fabrication of micro-optical and micro-electro-mechanical systems on a common substrate. This has led to new challenges in computer aided design of optical micro-electro-mechanical systems. We have extended our opto-electronic system CAD tool, Chatoyant, to attempt to meet the needs of optical MEMS designers. This paper presents new component models and analysis techniques which extend our tool to support optical MEMS design. We demonstrate these extensions with the analysis of a micro-optical high speed FFT engine and a 1x2 optical MEM interferometer switch.

Keywords: MEMS-CAD, optical MEMS, MOEMS, micro-optics

1. INTRODUCTION

Applications for optical MEMS (micro-electrical-mechanical systems) are growing to include scanning, projection, display, switching, printing, sensing, modulating, and data storage.[24] As these applications are quickly evolving from abstract ideas to marketable products, it is essential to have CAD tools to model these optical MEM systems in order to avoid costly prototyping. In this growing field, technologies are constantly advancing and CAD tools must be flexible in their ability to model and simulate new multi-domain components and systems.

We have created Chatoyant, a CAD tool that has been successfully used to design and simulate free space opto-electronic interconnect systems.[9,11,12] Chatoyant is a mixed signal CAD tool, capable of performing end-to-end system simulations while performing bit error rate (BER), insertion loss, crosstalk, and mechanical tolerancing analyses. Using Gaussian beam analysis of refractive optical components, Chatoyant provides sufficient accuracy for most macro-scale free space systems. However, to model optical MEM systems, Chatoyant must be extended to meet their specific concerns.

The role of optics in MEM systems is two-fold. First, MEM actuators can be used to precisely position micro-optical components that perform information processing tasks. Second, optics can be used to evaluate critical alignment and provide feedback on positioning of MEM components. Therefore, beyond functional design, optical MEMS CAD tools must simulate electrical, optical, and mechanical noise and support analysis for mechanical tolerancing.

With these criteria in mind, we have extended Chatoyant to model and simulate optical MEM systems. In order to model micro-optical systems, where wavelengths and physical dimensions are on the same scale, diffractive analysis models have been developed. Additionally, we have included a tolerancing analysis package for the precise alignment required for the correct operation of these systems.

In this paper, we present the extensions to Chatoyant that are used to model, simulate, and analyze optical MEM systems. We present models for refractive and diffractive components which are used as building blocks in optical MEM system design. We then focus on two optical MEM systems simulated with Chatoyant and present results that illustrate our model implementations and analysis techniques.

* Correspondence: Email: steve@ee.pitt.edu; WWW: http://kona.ee.pitt.edu/pittcad; Telephone: 412 648 9663; Fax: 412 624 8003

2. CAD TOOLS FOR OPTICAL MEMS

A complete optical MEMS CAD tool needs to model electrical and optical signals, mechanical positioning and tolerancing, thermal and vibration effects, fabrication, packaging, and, most importantly, the interaction of all these constraints. Currently, no single CAD tool completely models the complexity of optical MEM systems. Therefore, designers must use a collection of tools to model, simulate, and analyze each stage of this mixed signal design.

For conventional MEM design, a family of CAD tools is emerging, specializing in layout and simulation. Analogy has teamed with Microcosm Technologies to create a CAD package to design and simulate MEM systems through Analogy's Saber Tools.[2] Tanner markets MEMS Pro, which performs layout, error checking, and performance simulation through Tanner's T-Spice.[21] Both of these products use an analog electronic simulation backbone, forcing all system models into electrical templates. Universities have also created specialized tools for MEM modeling and simulation,[19,22,23] and have bridged the gap between CAD and foundry facilities.[8] Recently, new research has addressed the need to synthesize and optimize MEM systems.[16] However, no tools have begun to address the additional constraints imposed by micro-optical systems. This is the focus of our current work.

Built on top of Ptolemy[5], Chatoyant is a mixed-signal opto-electronic simulation framework. Chatoyant performs both static and dynamic simulations. Static simulations analyze mechanical tolerancing, power loss, insertion loss, and crosstalk, while dynamic simulations are used to analyze data streams with techniques such as noise analysis and bit error rate (BER) calculation. Until recently, Chatoyant has modeled light using only ray and Gaussian beam propagation methods.[11] These higher level abstractions are adequate for most refractive free-space opto-electronic systems. Chatoyant's optical library includes sources (vertical cavity surface emitting lasers, VCSELs, and multiple quantum well, MQW, modulators), optical components (lenses, lenslets, mirrors, apertures, etc.), as well as optical detectors. Opto-electronic signals are modeled using piece-wise linear discrete event techniques providing user control for accuracy and computation time.[13] Chatoyant possesses an advantage over other CAD tools by keeping all models and simulations within one internal framework.

In order to support micro-optical-electro-mechanical (MOEM) components, we have extended Chatoyant in three ways. First, we introduced modeling techniques for diffractive optics. This allows the use of diffractive models in cases where Gaussian approximations are not valid. Second, we have included models for micro-lenses, micro-mirrors, phase masks, and micro-mechanical actuators. This allows us to simulate complete MOEM systems in a single mixed signal framework. An additional requirement emphasized by these microsystems is support for tolerancing on the precise alignment required for desired operation. Therefore, our third extension is the implementation of a Monte Carlo tolerancing package within Chatoyant to determine worst case mechanical tolerancing and sensitivity.

In the next section, we present a brief background on refractive and diffractive lenses and our models based on scalar diffraction theory. We then move on to show the use of these and other micro-component models in system level simulations.

3. SCALAR WAVE MODELS FOR REFRACTIVE AND DIFFRACTIVE LENSES

In order to accurately model micro-optical systems, we must use scalar diffraction theory. This is for two reasons. First, the length scales of the components are on the same order as the wavelengths of light used. Second, MEMS technology lends itself to the creation of diffractive optical elements, such as Fresnel lenses, multiple level binary lenses, and computer generated holograms (CGHs). Examples of a refractive and diffractive lenses are given in Figure 1. In each case, the outline of a light beam striking the lens and converging to the focal point is added to the figure. The phase functions for each of the lenses are also given in Figure 1. These functions are multiplied by the complex wave function, used to describe the optical beam during diffraction analysis, to model a light wave propagating through a lens.

Refractive lenses act as a phase transformation, resulting when optical beams propagate through different indices of refraction. To model refractive lenses, we confine the lens' phase function with an aperture, usually circular. As seen by the equation found in Figure 1(a), the phase function of a refractive thin lens, p_{tl}, is dependent on the lens' focal length, f, and wave number, k. We note that even refractive lenses produce diffractive effects when the beam is clipped. Examples of this are shown later in this paper.

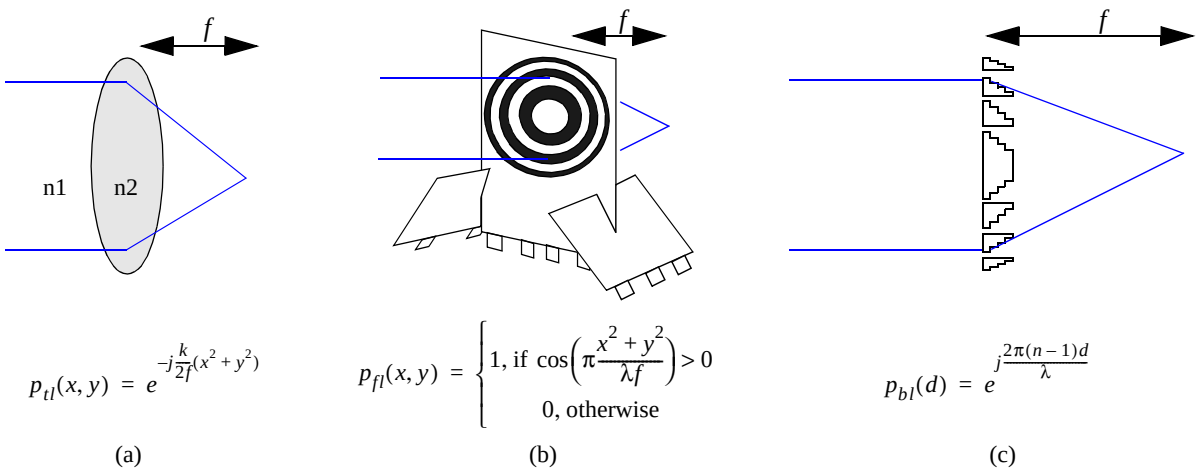

Figure 1: (a) Refractive Lens, (b) Diffractive Fresnel Lens, (c) Diffractive Multiple Level Binary Lens

On the other hand, diffractive lenses are designed to change both the light's intensity and phase, causing the light to interfere and form a focused spot. These lenses have advantages over standard refractive lenses in micro-optic systems. Through the fabrication of the diffractive lens, the focal length can be precisely defined within a wide range of numerical apertures, the thickness of the lens can be on the order of an optical wavelength, and the diameter can be on the order of tens of microns.[24]

A Fresnel lens, shown in Figure 1(b), is composed of bands of material that allow or restrict the propagation of the complex light wave. These diffracting rings affect the light wave such that the pattern acts as a spherical lens with an exact focal length. However, the efficiency of these lenses is very low and limited to approximately 10%. To simulate the lens, the transmission property of the rings are multiplied by the complex wave function. This transmission property can be thought of as a 0 (opaque band) or 1 (transparent band) phase function, as found in Figure 1(b).[18]

For the multiple level binary lens, shown in Figure 1(c), a phase change occurs based on the thickness of the lens. Since the lens is composed of varying thicknesses, we model this lens as a grid of phase masks, where each grid is has a constant thickness. The phase function of each grid, p_{bl}, is given in Figure 1(c), and is determined by the wavelength of the light, λ, the index of refraction, n, and the thickness of the material, d. The efficiency of these lenses is greater than the Fresnel lenses, but at a cost of a more complicated fabrication process.

Using these lens models, we determine how the scalar wave function propagates through a diffractive element. The result is based on the Huygens-Fresnel principle, that states that every unobstructed point of a wavefront at a given time serves as a source of spherical wavelets with the same frequency as the primary wave. Two approximations of the diffraction theory are the Fresnel and the Fraunhofer approximations.[4,6] The difference between the two approximations is the location of the observation plane, either in the near field (Fresnel approximation) or the far field (Fraunhofer approximation). With Fresnel diffraction, the curvature of the spherical waves is important to model, however, with Fraunhofer diffraction, the propagation distance is assumed to be large enough such that the spherical waves have spread into plane waves by the time they strike the observation plane. In the near field, as the observation screen moves away from the aperture, the diffractive image becomes more distinct, or structured. In the far field, as the observation screen moves from the aperture, the size of the image changes, not the shape.[7]

The Fraunhofer approximation can be calculated by a Fourier transform, rather than explicit integration techniques. Therefore, common FFT algorithms are used to solve for Fraunhofer scalar diffraction. In fact, most optical CAD tools perform this approximation rather than the Fresnel approximation, due to the simplicity of the Fourier transform. However, for micro-optical systems, we are often required to calculate the wave function in the near field. Therefore, we have chosen to use the more complex Fresnel approximation.

To compare our scalar diffraction models with experimental results, we simulate a free-space micro optical bench (FS-MOB) *4f* system using a 15° divergence angle, 850nm VCSEL source, two 250μm micro Fresnel lenses, and a 30μm square detector.

Chatoyant simulates the system by "placing" the system components on a substrate, assuming pre-alignment due to the fabrication technology, and analyzes the results. Our results match Motamedi et al.'s[15] experimental results in terms of both the lens efficiency (approximately 10%) and Gaussian shape (95% Gaussian). Using similar techniques we have modeled other diffractive components, such a apertures, computer generated holograms (CGH), and micro-mirrors.

4. SIMULATIONS AND ANALYSES OF OPTICAL MEM SYSTEMS

In this section, we present results from the simulation and analysis of two optical MEM systems. The first contains no moving parts, but has critical tolerancing requirements. We show how we use scalar diffractive modeling and Monte Carlo analysis to analyze the mechanical tolerances of the system. The second system is a dynamic optical MEM system used for mechanical switching of arrays of optical data. We use this system to show Chatoyant's ability to model a mixed system of mechanical MEMs, optics, and electronic feedback.

4.1. High Speed FFT Micro-optical system

We are part of a team designing, building, and analyzing micro-optical systems, with our current project being an optical MEM system performing a high speed FFT, shown in Figure 2. This system can be used for the implementation of real-time adaptive signal processing systems, and has motivated our diffractive analyses. In this section, we present simulations and analyses of the system using Chatoyant.

The system is based on integrating a compact optical system, called the Optical Transpose Interconnect System (OTIS)[3], together with two functional logic blocks. The logic blocks perform the necessary computations, and the optics perform a butterfly shuffle. Each logic block is composed of a stack of 16 CMOS processor dice, bonded in a substrate-insulation-substrate sandwich, creating a cube. Bonded to the edge of the processor stack, is the GaAs opto-electronic sub-system. Since the system is bi-directional, each stack has extra circuitry to drive the optical VCSEL sources and amplify the received data from the photodetectors. The sources and detectors are placed in a 16 x 16 array that allows parallel data transmission. The components are placed onto a silicon microbench, and are held and aligned using MEM technology.

4.1.1. VCSEL Mechanical Tolerancing

We simulate the optical sub-section of the high speed FFT system to determine the mechanical tolerancing of the VCSEL positions. As seen in Figure 2, this sub-system starts with a 15 degree divergence VCSEL array. These source beams propagate 508 μm though a sapphire substrate to a lenslet array, where each lenslet has a 250μm diameter and radius of curvature of 0.145mm. The beams then propagate 2 cm through free-space to another lenslet array, which is backed by another 508 μm sapphire substrate, and are finally received by 80 μm square detectors. In this following example, we monitor only one beam of the VCSEL array.

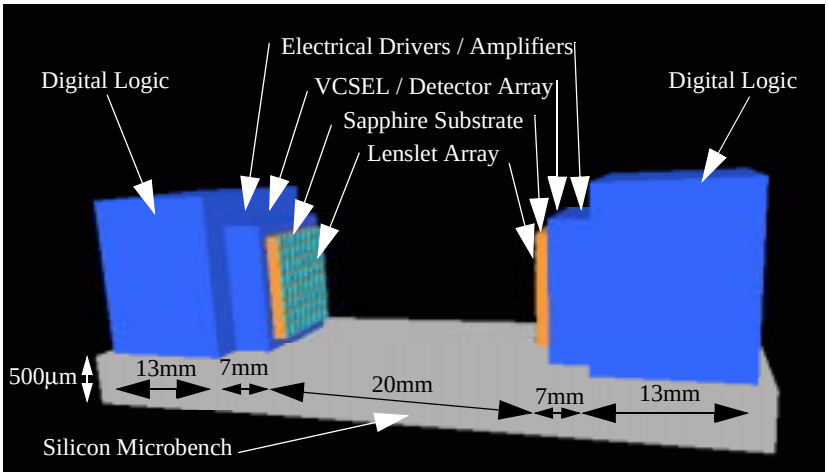

Figure 2: FFT Optical MEM System

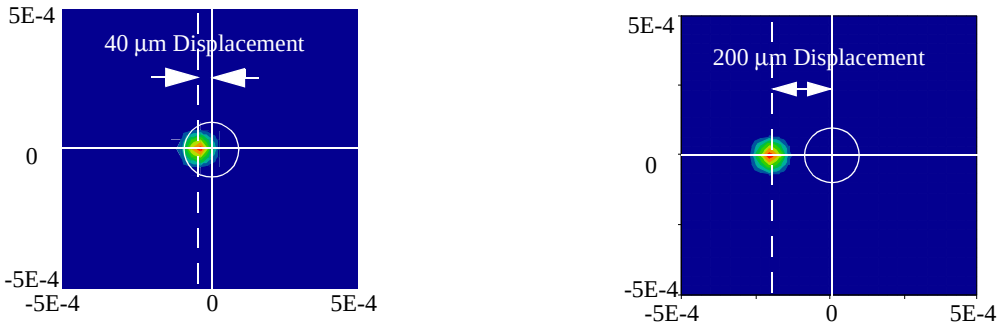

(a) 1µm Source Offset (b) 5µm Source Offset

Figure 3: Intensity Contours of a VCSEL Offset (a) 1µm and (b) 5µm Propagated to the Second Lenslet

To simulate the VCSEL positional tolerancing, the sources are offset in the *x* direction, causing off-axis clipping between the beam and the first lenslet. Therefore, scalar diffractive models have to be used since there are no simple Gaussian approximation models for off-axis clipping. Figure 3 shows the intensity contours for an offset VCSEL beam that has propagated through the first lenslet to the second lenslet. Figure 3(a) shows the contour image of a VCSEL offset 1 µm in the *x* direction, and Figure 3(b) shows the intensity contour of a VCSEL offset by 5 µm. With such small offsets, the clipping at the first lenslet is almost identical to the case for no offset. At the first lenslet plane, a power loss of 4.53% is found with no offset in the VCSEL source. The same power loss is found for a 1 µm offset, and a power loss of 4.54% for a 5 µm VCSEL offset. As the light propagates to the second lenslet, the positional displacement of the 1 µm offset beam grows to approximately 40µm, as seen in Figure 3(a). The approximate size and position of the second lenslet are superimposed on the contour graphs. Most of the beam passes through the second lenslet, although, 22.6% of the remaining power is lost, resulting in a total system insertion loss of 26.1%. Figure 4 shows the *x*-axis intensity distribution at the 80 µm detector. The shape of the beam is no longer Gaussian, as visible side lobes are present. Note that the lens has steered the beam back onto the detector, with the center of the beam shifted off-axis only 1 µm. Also, note that the side lobes are almost at the full radius of the detector, therefore, for some cases, these lobes will miss the detector, resulting in even a greater insertion loss. Figure 3(b) shows the positional displacement of the 5 µm offset beam is almost 200 µm at the second lenslet. With such a large axial offset, the beam misses the second lenslet, and the signal never reaches the detector. This illustrates the need for critical alignment tolerances in these micro-optical systems.

In general, it is hard to predict what cases or offsets will give the worst case behavior in a complex system. Therefore, a standard technique is to use Monte Carlo simulations[17], which vary the mechanical properties (position and orientation) of each of the components according to a probability distribution based on manufacturing tolerances, mechanical vibration, and thermal expansion. We discuss our extensions to Chatoyant supporting this analysis in the next section.

4.1.2. Monte Carlo Analysis

We have enhanced Chatoyant to allow the designer to use probability distributions (e.g., linear, Gaussian, or Poisson) instead

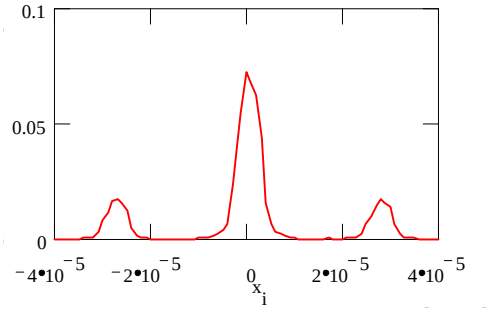

Figure 4: Scalar Intensity Distribution at the 80 µm Detector

of specific values for component parameters. During Monte Carlo simulation, Chatoyant runs the system multiple times using these distributions for parameter values and returns the system parameters of the best and worst sets of parameters.

As an example, the same sub-system as before is simulated using Chatoyant's Monte Carlo analysis. In this simulation, the VCSEL positions are held constant as a reference geometry for the system, and the parameter ranges for the other components are given in the first row of Table 1. There are ten tolerancing parameters in the system, making sensitivity analysis of the individual parameters to the system performance difficult. After running the Monte Carlo analysis for 10,000 random simulations, we analyze which cases have the largest deviation in parameters, but detect full optical power, and the cases where the parameters deviate the least, but result in the beam entirely missing the desired detector. The 10,000 random simulations with 10 degrees of freedom completed in about 80 minutes, running on a 300 MHz machine running Linux. We examine the runs in which full power is detected (1,790 out of 10,000 runs), sort them by maximum parameter deviation, and report the top two cases in Table 1 (Full Power #1 and #2). Similarly, we examine the runs in which at least one beam completely missed its desired detector (6,777 out of 10,000 runs), sort these in terms of minimum parameter deviation, and report the top two (No Power #1 and #2). When the beam completely misses the detector, we conclude the most common cause is the tilts (ρ or θ) of the lenses. This is shown in Table 1 by the largest normalized parameter in each run, typed in bold, being a lens tilt. Notice, for most parameters, the offsets of the runs Full Power #1 and #2 are larger than the parameter offsets for No Power #1 and #2. This is due to the system parameters compensating for each other. That is, if one parameter steers the beam out of the optical path, another parameter compensates by steering the beam back in line.

Table 1: Monte Carlo Analysis Results

Parameter	Lens1_x (μm)	Lens1_y (μm)	Lens1_ρ (°)	Lens1_θ (°)	Lens2_x (μm)	Lens2_y (μm)	Lens2_ρ (°)	Lens2_θ (°)	Detect_x (μm)	Detect_y (μm)
Range	±1	±1	±0.05	±0.05	±1	±1	±0.05	±0.05	±1	±1
Full Power #1	.483923	.795798	.029097	.044562	.792757	-.625983	-.037319	.036576	-.655080	-.432245
Full Power #2	.792841	.596940	.042626	.042072	-.644088	.938024	.049612	.020996	.427233	-.938518
No Power #1	.422470	.080384	**-.023795**	.023149	-.431848	.403542	-.012593	.000738	.009119	.028665
No Power #2	.045314	-.411032	-.019199	.024634	.128980	.208934	-.016890	**-.027808**	-.168906	-.031077

4.2. 1x2 Optical Switch

Our second example system is a 1x2 optical MEM switch, based on two interferometers. An interferometer works by an input source beam being split into two, the optical path length of the two beams being altered, and the beams being recombined. The resulting beam appears "on" or "off" due to constructive or destructive interference during the recombination of the beams. For our 1x2 switch, the input beam is split in two, resulting in two inputs for two interferometers, as can be seen in Figure 5.

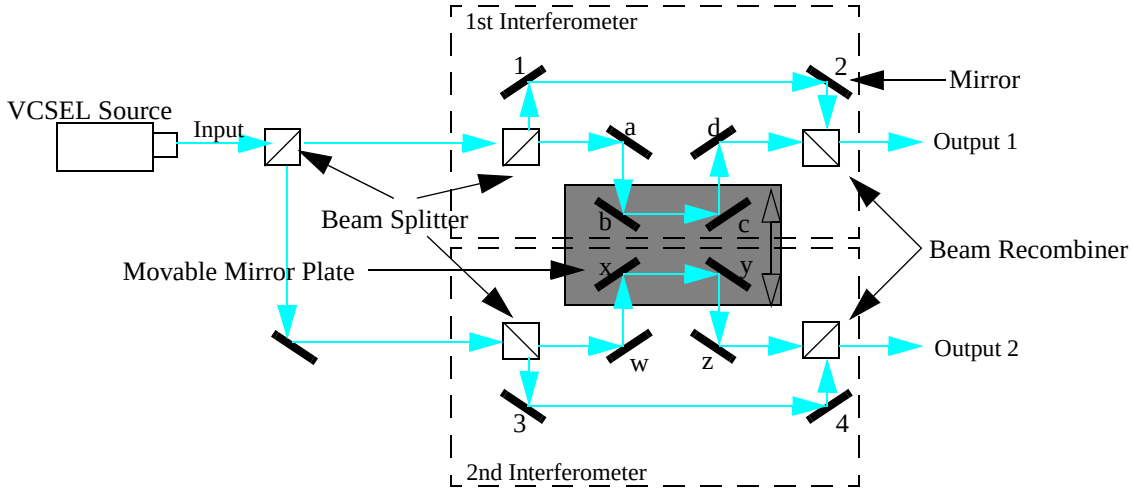

Figure 5: Two Interferometers and the Mirror Plate

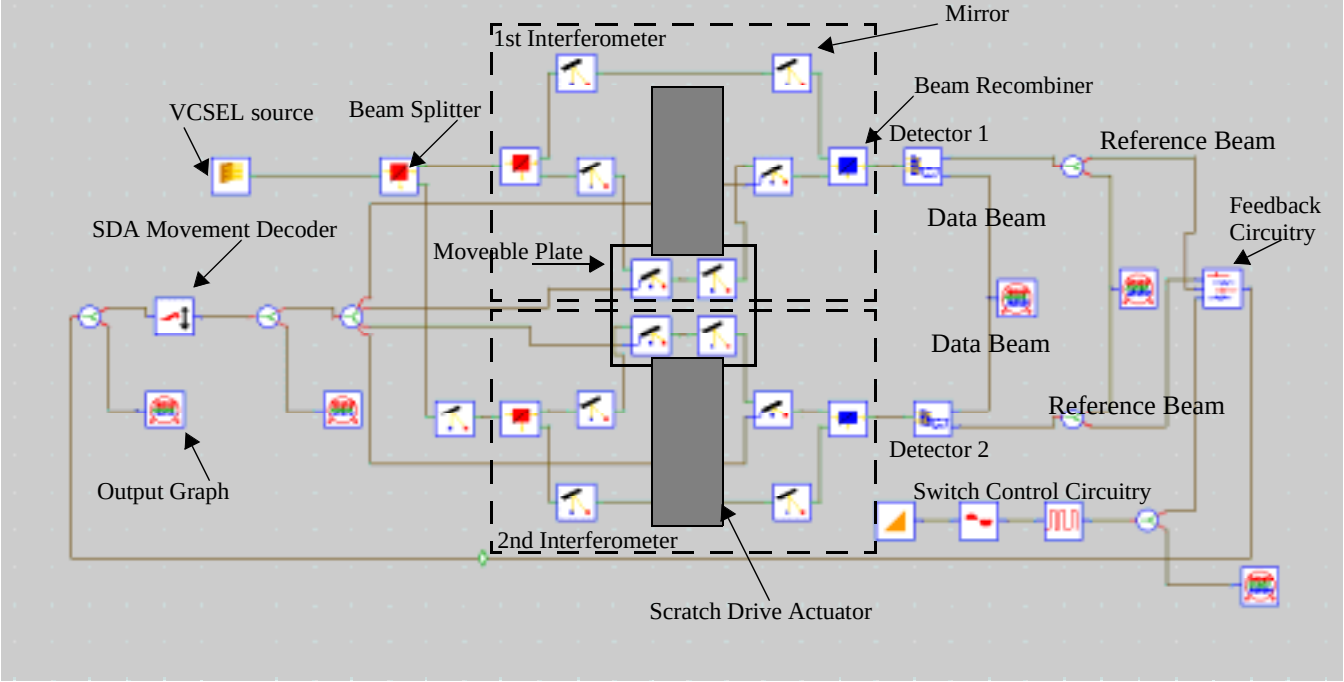

Figure 6: 2x1 Switch Described in Chatoyant

Both interferometers (beam splitter, mirrors, and beam recombiner) are boxed by a dashed line in Figure 5. The first interferometer compares the path length through mirrors 1-2 to the path length through mirrors a-b-c-d, and the second interferometer compares the path length through mirrors 3-4 with the path length through mirrors w-x-y-z, all shown with light arrows. A movable plate on the substrate of the wafer holds two of the mirrors from each path (b, c and x, y) in the shape of an "X". The position of the plate is controlled by feedback circuitry in the system, and is moved by two scratch drive actuators (SDA) sets[1], which move the mirror plate back and forth. These mirrors control the optical path lengths through mirrors a-b-c-d and w-x-y-z. Therefore, when the plate moves, the optical path length of one interferometer is shortened causing constructive interference on one detector, while the other optical path is lengthened, causing destructive interference. The components are created using surface micromachined technology. With this technology, free-space micro-bench components can be fabricated "out of plane", or normal to the surface, and pre-aligned during the fabrication of the devices, and post-aligned with micro-positioners.

The 1x2 switch, as described in Chatoyant, is shown in Figure 6. In Chatoyant, each icon represents a component model, written in C++, with sets of parameters defining the characteristics of the component. Each line represents a signal path (either optical or electrical) connecting the outputs of one component to the inputs of the next. Several of the icons, such as the *VCSELs*, *Beam Splitters*, and *Mirrors*, model the opto-electronic components themselves, while others, such as the *Output Graph*, are used to monitor and display the behavior of the system.

In Figure 6, each interferometer is again boxed by a bold dashed line. The movable plate, holding the four mirrors, is also shown by the solid, bold box. Both scratch drive actuators are shown by the lined, rectangular boxes. The plate and the SDA are not directly drawn in Chatoyant, since they are modeled as signals altering the optical paths. We have added them to the figure for clarity. As shown, a 3x3, VCSEL array source is split into two beam arrays, providing inputs into the two interferometers. The optical path lengths through mirrors 1-2 and 3-4 are 3mm, with the mirror plate adjusting the path lengths through mirrors a-b-c-d and w-x-y-z. The number of mirrors that steer the beams through the system affects the insertion loss of the output beams, since we assume each gold plated mirror has an efficiency of 87%.[24] We assume our beam splitter to be ideal (50%/50%). A spot size of 80μm is required such that no lenses have to be added to the system to keep the beams from significantly diverging and becoming unfocused.

The SDAs are modeled in Chatoyant by the actuator's "step" size (determined by the height and length of the actuator) and the voltage pulse train, which drives the actuator.[1] A scratch drive actuator is shown in Figure 7(a). A voltage causes electrostatic attraction between the SDA plate and the substrate, as shown by the hollow arrows in Figure 7(b). With this attraction, the

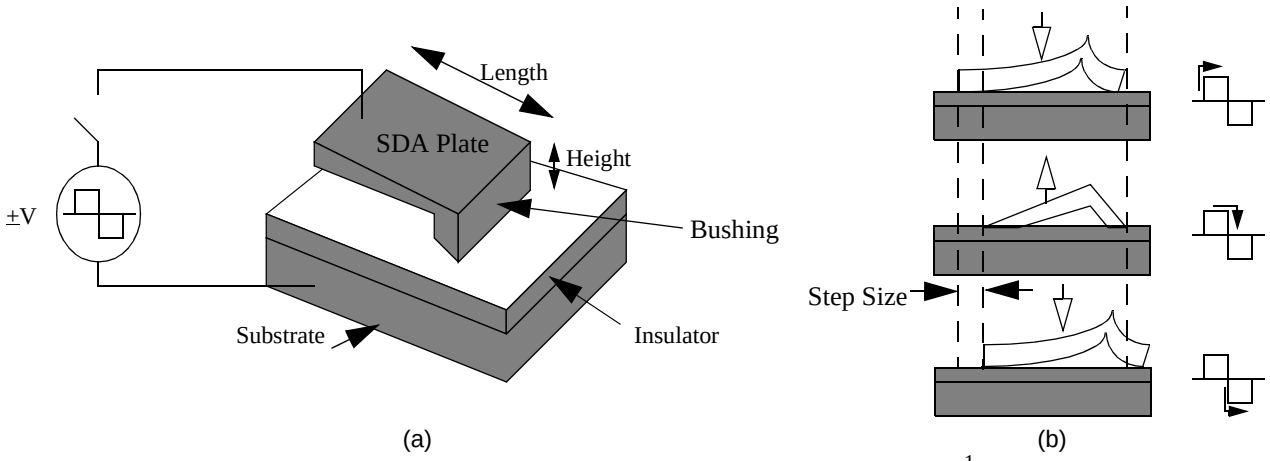

Figure 7: (a) Scratch Drive Actuator (SDA) (b) Step Movement[1]

bushing is stretched forward, and with the pulsing action, the SDA regains shape, causing the plate to move forward a step. In this simulation, the SDAs are powered by a 50kHz pulse with an amplitude of ±70 V, and a height and width resulting in a 11nm "step" size.[20] Two actuators are needed to move the mirror plate, one for each direction, and are controlled by electronic feedback circuitry that specifies which actuator, if any, should crawl. Since we are using a 3x3 array of VCSEL sources, one beam is used as a reference and is always "on", as shown in the upper left corner of Figure 8. This beam is detected and compared with the desired value in the feedback circuitry. The other 8 beams are used for data transfer. The feedback circuitry is a basic comparator, which compares the converted voltage from the designated detector with a threshold voltage, specified by the user. If the received voltage is not at the desired level, the actuator keeps moving the mirrors to a position that produces the correct interference, resulting in the correct optical power at the desired detector.

4.2.1. Static Simulations

We first present static simulations, useful for determining system insertion loss, efficiency and crosstalk. The two interferometers have different efficiencies. Figure 8 shows a Chatoyant output image at one of the 3x3 detector arrays. For Detector 1, Chatoyant reports a worst case efficiency of approximately 52% for one of the beams in the array. 23% of the power is lost due to the efficiency of the mirrors, and an additional 25% of the power is lost is due to the beams' divergence and the detector sizes. With the longer optical propagation and the extra mirror, Detector 2's efficiency drops to approximately 41%. As shown in Figure 8, the detector size and spacing also generates optical system crosstalk. Worst case crosstalk between neighboring detectors is measured at -9.5 dB.

4.2.2. Dynamic Simulations

The second type of simulations performed are dynamic simulations, where streams of data pass though the switch to the specified detectors. Figure 9 shows five outputs from a single simulation of the switch in Chatoyant. Figure 9(a) shows a 1.6 kHz

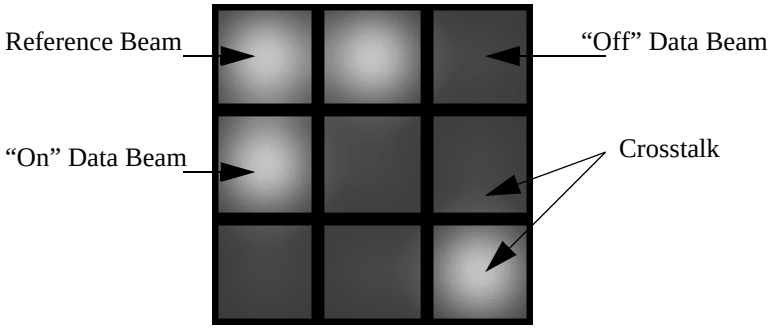

Figure 8: Detector Output Array

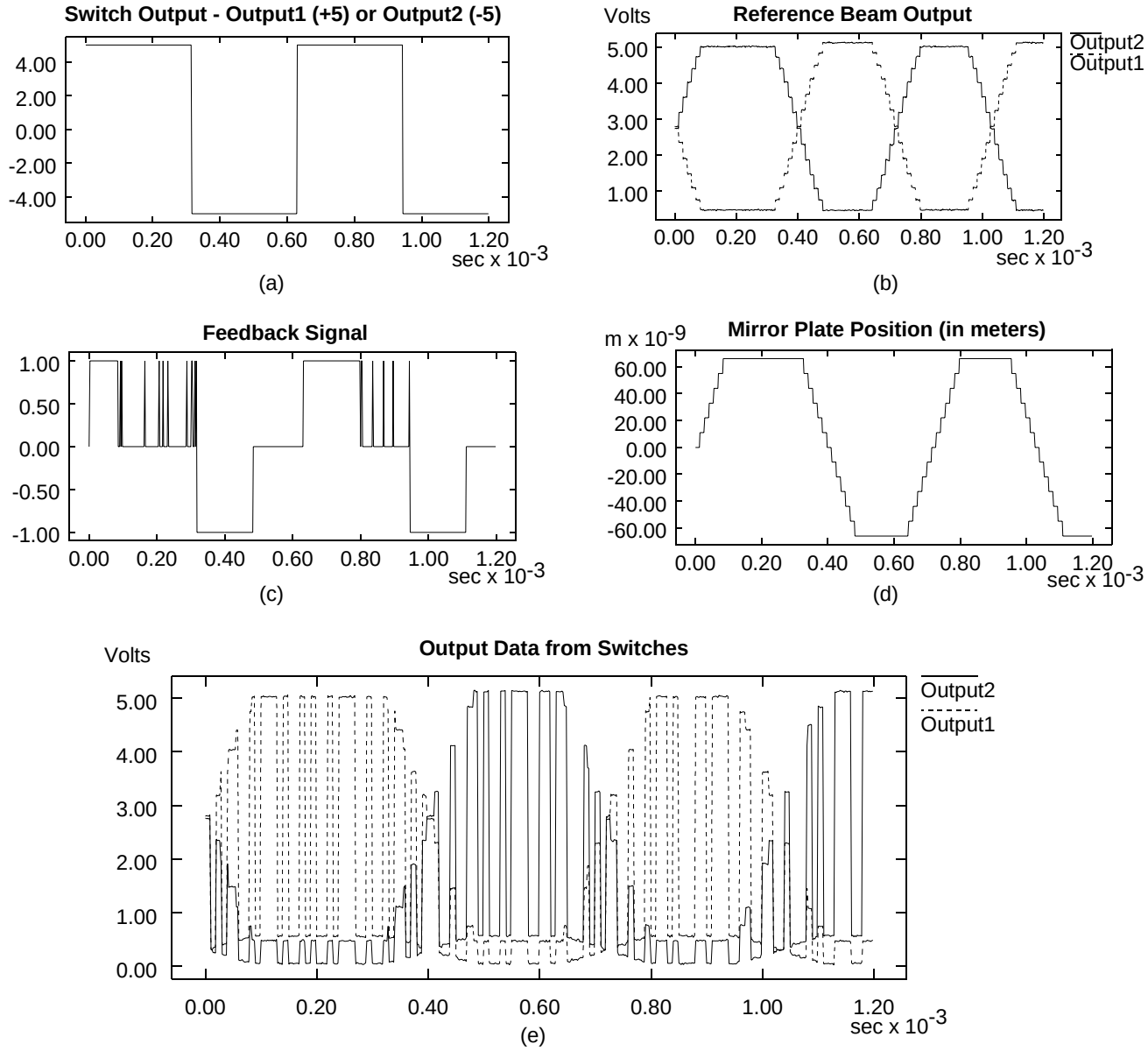

Figure 9: Dynamic Response of the 2x1 Optical MEM Switch

square wave, which selects the switch's output. When the value is positive, Output 1 is selected, and when the value is negative, Output 2 is selected. Figure 9(b) shows the detected voltage output of the reference bit. The optical detectors are composed of p-i-n photo diodes, which convert optical power into current, and a transimpedance amplifiers, which convert the current to voltage. Figure 9(c), shows the output of the comparator circuity, which controls the SDAs. If the output is positive, the SDAs moves the mirror plate reducing the optical path of the first interferometer, while increasing the optical path of the second interferometer. If the output is negative, the other SDAs moves the mirror plane in the opposite direction. If the output is zero, neither of the SDAs move, resulting in no mirror movement. Optical feedback allows us to compensate for mechanical tolerancing and noise. The noise changes the reference output voltage, occasionally causing the feedback circuity to signal the SDA to move another step. This accounts for the "spikes" that are found in Figure 9(c). Figure 9(d) shows the movement of the mirror plate. Recall the mirror plate moves up and down by the step size of the actuators. The spikes seen in Figure 9(c) do not move the SDAs since a 50 kHz voltage pulse can not be completed in such a short time. The final graph, Figure 9(e), shows one stream of data that is passed from one VCSEL source, through the interferometers, to the desired switch output. Both outputs from the switch are shown in the same graph, the first output by a dashed line, and the second out-

put with a solid line. In this example, the optical data stream is passing at only 125 kbits/sec. In a real application, the optical signal would actually be at a much higher bit rate (300 MHz - 3 GHz), but is kept slow here for illustration purposes. In this example, for each switching pulse, approximately 50 bits are passed through to the receiver. In reality, we would switch packets of 10^3 - 10^5 bits. Similarly, we show data bits during the switch transition, while in real systems "guard bands" would be added to the data stream.

In theory, with a 50 kHz clock driving the SDAs, the actuators will take 10 μsec to move each of the 11nm steps. With a 850 nm laser source, the optical paths in the interferometer differ by 212.5 nm between complete constructive and destructive interference. For worst case switching time, the movable mirror plate, would have to move this entire distance. With a step size of 11nm, this would take approximately 20 steps, resulting in a switching time of 200 μsec.

However, in simulation, we find that with the detector parameters and the feedback circuity voltage reference specified, the maximum number of steps the SDA is moving is only 12, resulting in a switching time of 120 μsec. This is because neither total constructive or destructive interference is achieved. This is visible in Figures 9(b) and (e), with the "off" switch output not completely reaching 0 volts. Total interference could be reached at the cost of increased switching time, by altering the feedback circuitry parameters. Using Chatoyant's BER analysis[11], the designer can perform trade-offs between BER, switching time, and mechanical tolerancing to achieve the desired system performance.

Using parameters from the published literature, the free space interferometer switch that we have modeled here is comparable to optical fiber switches built by Lee and Marxer. Worst case switching time of Lee, et al.'s[10] surface-micromachined, moving plate mirror, fiber switch was found to be between 10 and 15 msec, and Marxer et al.[14], using bulk-micromachining and a comb-drive reports a switching time of 200 μsec.

5. SUMMARY AND CONCLUSIONS

Optical MEMS have the potential of drastically reducing the size and cost of digital communications and computation systems. However, due to the multiple technologies (optical, electrical, and mechanical) utilized in optical MEM systems, complete optical MEM CAD tools are difficult to create. This paper has shown the extensions, in particular the diffractive models and mechanical tolerancing using Monte Carlo analysis, that have been added to Chatoyant to enable the modeling of micro-optical-electro-mechanical systems.

Chatoyant's ability to perform and analyze optical, electrical, and mechanical trade-offs make our system valuable to optical MEM designers. Keeping all the simulations internal to the Chatoyant framework allows for quick and efficient analysis throughout multiple domains. Results from system simulations show that Chatoyant is a useful, practical alternative to costly prototyping optical MEM systems.

ACKNOWLEDGMENTS

We would like to acknowledge the support of DARPA contract number F3602-97-2-0122 and NSF grant ECS-9616879. We also thank Dr. Tamal Mukherjee for his helpful discussions.

REFERENCES

1. Akiyama, T., Collard, D., Fujita, H., "Scratch drive actuator with mechanical links for self-assembly of three-dimensional MEMS," *Journal of Microelectromechanical Systems*, Vol. 6, No. 1., March 1997, pp. 10-17.
2. "Analogy and Microcosm Technologies Announce MEMS Solution", Analogy Press Release, Raleigh, North Carolina, June 15, 1998.
3. Blume, M., Marsden, G.C, Marchand, P.J., Esener, S.C., "Optical Transpose Interconnect System for Vertical Emitters," *OSA Topical Meeting on Optics in Computing*, Lake Tahoe, NV, March 1997, pp. 233-235.
4. Born, M., Wolf, E., *Principles of Optics*, (Pergamon Press, 1959).
5. Buck, J., Ha, S., Lee, E.A., Messerschmitt, D., "Ptolemy: a framework for simulating and prototyping heterogeneous systems," *Int. J. Computer Simulation*, Vol. 4, 1994, pp. 155-182.
6. Goodman, J.W., *Introduction to Fourier Optics*, Second Edition (The McGraw-Hill Companies, Inc., 1996).

7. Hecht, E., *Optics*, Second Edition (Addison-Wesley Publishing Company, 1987).
8. Karam, J.M., Courtois, B., Boutamine, H., Drake, P., Rencz, M., Poppe, A., Székely, V., Hofmann, K., Glesner, M., "CAD and foundries for microsystems", *Proceedings of the 1997 Design Automation Conference*, Anaheim, CA, June 1997, pp. 674-679.
9. Kurzweg, T.P., "A CAD system for modeling free space opto-electronic systems," M.S. Thesis, (Department of Electrical Engineering, University of Pittsburgh, Pittsburgh, PA., 1997).
10. Lee, S.S., Motamedi, E., Wu, M.C., "Surface-micromachined free-space fiber optic switches with integrated microactuators for optical fiber communication systems," in *Proceedings of the 1997 International Conference of Solid-State Sensors and Actuators (TRANSDUCERS 97)*, 1997, paper 1A4.07P.
11. Levitan, S.P., Kurzweg, T.P., Marchand, P.J., Rempel, M.A., Chiarulli, D.M., Martinez, J.A, Bridgen, J.M., Fan, C., McCormick, F.B., "Chatoyant: a computer-aided design tool for free-space optoelectronic systems," *Applied Optics*, Vol. 37, No. 26, September, 1998, pp. 6078-6092.
12. Levitan, S.P., Marchand, P.J., Kurzweg, T.P., Rempel, M.A., Chiarulli, D.M., Fan C., McCormick, F.B., "Computer-Aided Design of Free-Space Opto-Electronic Systems," *Proceedings of the 1997 Design Automation Conference*, Anaheim, CA, June 1997, Best Paper Award, pp. 768-773.
13. Martinez, J.A., Levitan, S.P., Chiarulli, D.M., "Piecewise Linear Large Scale Models for Optoelectronic Devices," *OSA Topical Meeting on Optics in Computing*, Aspen, CO, April 1999.
14. Marxer, C., Gretillat, M.-A., de Rooij, N.F., Battig, R., Anthamatten, O., Valk, B., Vogel, P., "Vertical mirrors fabricated by reactive ion etching for fiber optical switching applications," *Proceedings of the 10th Workshop of Micro Electro Mechanical Systems (MEMS)*, Nagoya, Japan, 1997, pp. 49-54.
15. Motamedi, M.E., Wu, M.C., Pister, K.S.J., "Micro-opto-mechanical devices and on-chip optical processing," Optical Engineering, Vol. 36, No. 5, May 1997, pp. 1282-1297.
16. Mukherjee, T., Fedder, G.K., "Structured Design Of Microelectromechanical Systems," *Proceedings of 34th Design Automation Conference Anaheim, CA*, June 1997, pp. 680-685.
17. Rubinstein, R.Y., *Simulation and the Monte Carlo Method*, (John Wiley & Sons, 1981).
18. Saleh, B.E.A., Teich, M.C., *Fundamentals of Photonics* (New York: Wiley-Interscience, 1991).
19. Senturia, S. D., "CAD for Microelectromechanical Systems," *Proceedings of the 1997 International Conference of Solid-State Sensors and Actuators (TRANSDUCERS 95)*, Stockholm, Sweden, June 1995, Vol. 2, Paper No. 232-A7.
20. Su, G.D., Lin, L.Y., Wu, M.C., "Single-chip femtosecond autocorrelator realized by surface-micromachined integrated optics," *Conference of Lasers and Electro-Optics (CLEO)*, Baltimore, MD, 1997, paper CWL2.
21. Tanner Research, Inc. "http://www.tanner.com/eda/products/memspro.htm"
22. Vandemeer,J.E., "Nodal Design of Actuators and Sensors (NODAS)", M.S. Thesis, (Department of Electrical and Computer Engineering, Carniege Mellon University, Pittsburgh, PA., 1997).
23. Wilson, N.M., Hsiau, Z.K., Dutton, R.W., Pinsky,P.M., "A Heterogenous Environment for Computational Prototyping and Simulation Based Design of MEMS Devices", *SISPAD 98*, Leuven, Belgium, Sept. 2-4, 1998.
24. Wu, M.C., "Micromachining for optical and Optoelectronic Systems," *Proceedings of the IEEE*, Vol. 85, No. 11, (November 1997), pp. 1833-1856.